Synthesis, characterization, antibacterial and antitumoral activities of mononuclear zinc complexes containing tridentade amine based ligands with N3 or N2O donor groups

Christiane Fernandes, Adolfo Horn Jr, Olney Vieira-da-Motta, Milton M. Kanashiro, Michelle R. Rocha, Rafaela O. Moreira, Samila R. Morcelli, Bruna F. Lopes, Luciana da S. Mathias, Franz V. Borges, Layla J.H. Borges, William R. Freitas, Lorenzo C. Visentin, João C.A. de Almeida, Gerhard Schenk

PII: S0020-1693(14)00143-1
DOI: http://dx.doi.org/10.1016/j.ica.2014.02.040
Reference: ICA 15898

To appear in: *Inorganica Chimica Acta*

Received Date: 15 August 2013
Revised Date: 14 February 2014
Accepted Date: 26 February 2014

Please cite this article as: C. Fernandes, A. Horn Jr, O. Vieira-da-Motta, M.M. Kanashiro, M.R. Rocha, R.O. Moreira, S.R. Morcelli, B.F. Lopes, L.d.S. Mathias, F.V. Borges, L.J.H. Borges, W.R. Freitas, L.C. Visentin, J.C.A. de Almeida, G. Schenk, Synthesis, characterization, antibacterial and antitumoral activities of mononuclear zinc complexes containing tridentade amine based ligands with N3 or N2O donor groups, *Inorganica Chimica Acta* (2014), doi: http://dx.doi.org/10.1016/j.ica.2014.02.040

Synthesis, characterization, antibacterial and antitumoral activities of mononuclear zinc complexes containing tridentade amine based ligands with N3 or N2O donor groups

Christiane Fernandes [a,*], Adolfo Horn Jr [a], Olney Vieira-da-Motta [b], Milton M. Kanashiro [c], Michelle R. Rocha [a], Rafaela O. Moreira [a], Samila R. Morcelli [a], Bruna F. Lopes[a], Luciana da S. Mathias [b], Franz V. Borges [c], Layla J. H. Borges [c], William R. Freitas [c], Lorenzo C. Visentin [d], João C. A. de Almeida [e] and Gerhard Schenk [f]

[a]*Laboratório de Ciências Químicas, Universidade Estadual do Norte Fluminense Darcy Ribeiro, 28013-602, Campos dos Goytacazes/RJ, Brazil.*

[b]*Laboratório de Sanidade Animal, Universidade Estadual do Norte Fluminense Darcy Ribeiro, 28013-602, Campos dos Goytacazes/RJ, Brazil.*

[c] *Laboratório de Biologia do Reconhecer, Universidade Estadual do Norte Fluminense Darcy Ribeiro, 28013-602, Campos dos Goytacazes/RJ, Brazil.*

[d] *P&D NanoBusiness e-Diffraction Pharma, CEP: 22451-900, Rio de Janeiro/RJ, Brazil.*

[e]*Laboratório de Fisiologia e Bioquímica de Microrganismos, Universidade Estadual do Norte Fluminense Darcy Ribeiro, 28013-602, Campos dos Goytacazes/RJ, Brazil.*

[f] *School of Chemistry and Molecular Biosciences, The University of Queensland, Brisbane, QLD 4072, Australia.*

To whom correspondence should be addressed: Phone: +55 22 2739 7213. Fax:+55 22 2739 7046. E-mail: chrisf@uenf.br

Abstract

The synthesis and characterization of the four zinc(II) complexes $[Zn(HL_1)Cl_2]$ **(1)**, $[Zn(H_2L_2)Cl_2]$**(2),** $[Zn(H_2L_3)Cl_2]$ **(3)** and$[Zn(H_2L_4)Cl_2]$ **(4)**, where HL_1= (bis-2-pyridylmethyl)amine, H_2L_2= (2-hydroxybenzyl-2-pyridylmethyl)amine, H_2L_3= N-2[(pyridine-2-ylmethyl)amino)ethanol, H_2L_4= 1-[(pyridine-2-ylmethyl)-amino]-propan-2-ol are reported; **(3)** and **(4)** are new while **(2)** was reported previously but its structure had not been determined. The complexes were characterized by elemental analysis, IR, UV-Vis and NMR spectroscopies, electrospray ionization mass spectrometry (ESI(+)-MS) and tandem mass spectrometry ESI(+)-MS/MS). X-ray diffraction studies were performed for complexes **(1)-(3)** revealing the presence of mononuclear structures in the solid state. The x-ray analyses of **(1)** and **(3)** demonstrate that HL_1 and HL_2 act as tridentate ligands, while the ligand H_2L_2 in **(2)** is bidentate. The cytotoxic properties of the ligands and of all the complexes were examined using human leukemia THP-1, U937 and Molt-4 cells. Complex **(4)** exhibited the highest cytotoxicity in this series with an IC_{50} value of 75 ± 1 µmol L^{-1} against U937 cells. Transmission electron microscopy (TEM) reveals ultrastructural changes typical of apoptotic cells. The induction of apoptosis was confirmed by the annexin V assay. The antimicrobial activity of complexes **(1)-(4)** was also investigated *in vitro* against four Gram-positive bacteria (ATCC10832, ATCC25923, COL) and the clinical *Staphylococcus aureus* isolate LSA88 (SEC/SEF/TSST-1+). Complex **(2)** showed the most potent inhibitory activity, reaching almost 100% of inhibition against all strains tested. Morphological investigations using TEM indicate that the antibacterial activity of complex **(2)** may be associated with the inhibition of cell wall and therefore cell division.

Keywords: Mononuclear Zn complexes; ESI(+)-MS/MS; Crystal structure; Antibacterial activity; Cytotoxic activity; Transmission electron microscopy (TEM).

E-mail: chrisf@uenf.br Fax: +55 22 2739 7046. Phone: +55 22 2739 7213.

1. Introduction

Zinc has a vital importance in metabolism, being required for proper functioning of the immune system, the formation of red blood cells, organ, muscle and bone function, cell membrane stability, as well as cell growth, division, differentiation and genetics [1]. Zinc compounds are employed as radioprotective agents [2], tumor photosensitizers [3], antidiabetic insulin mimetics [4] and antimicrobial agents [5,6,7]. In 2012, Muthmary and co-workers reported the cytotoxicity of di-zinc(II) complexes for human hepatoma HepG2 cancer cells, where these compounds were able to induce caspase-dependent apoptosis [8]. In 2013, Kessissoglou and co-workers reported the antimicrobial activity of zinc(II) complexes on five different microorganisms with IC_{50} values in the range of 1-4 $\mu g.ml^{-1}$ [9]. Another established application for a zinc compound is as an anti-dandruff agent; zinc pyrithione (ZPT) is an antimicrobial compound used since 1960 in anti-dandruff shampoos and also anti-fouling paints [10]. In 2011, Saunders and co-workers reported that the ZPT efficacy against fungi is related to both the increasing concentrations of intracellular copper and the inactivation of Fe-S cluster-containing proteins [11].

Recently, we reported the antibacterial activity of iron(III), cobalt(II), copper(II) and zinc complexes, obtained with the ligand (N-(2-hydroxybenzyl)-N-(2-pyridylmethyl)[(3-chloro)(2-2-hydroxy)]propylamine), against nine strains of *S. aureus*. Complexes containing cobalt and zinc showed the most potent inhibitory activity, reaching almost 100% of inhibition against the nine strains under investigation. Based on TEM studies, it was proposed that the zinc complex interacts directly with the genetic material of the *S. aureus* cells, promoting cell wall and cytoplasmic membrane damages, which result in the leakage of cellular content and inhibiting further division processes [12]. In that study, the metal ions were coordinated by tetradentate ligands which provide a pyridine, a phenol, an alcohol and a tertiary amine as coordinating groups. Due to the encouraging results obtained

with the zinc complex, we decided here to investigate simpler ligands, i.e. the tridentate bipodal ligands HL1= (bis-2-pyridylmethyl)amine, H2L2= (2-hydroxybenzyl-2-pyridylmethyl)amine, H2L3= N-2[(pyridine-2-ylmethyl)amino)ethanol and H2L4= 1-[(pyridine-2-ylmethyl)-amino]-propan-2-ol). We also aimed to identify structural features related to the antibacterial activity of the corresponding zinc complexes. Furthermore, we also investigated the antitumor activity of these zinc complexes to probe a possible connection between these two biological activities. It is worth noting that complex **(1)**, the crystal structure of which is reported in this manuscript, was recently identified as an inhibitor of the activated RAS protein [13]. In cancer research RAS represents a target of high interest owing to its critical involvement in about 30% of all human malignancies [14].

2. Experimental

2.1 Materials and methods

All the reagents and solvents were commercially available of high purity and used as such. The CHN elemental analysis for the complexes was performed on a Thermo Scientific FLASH 2000 CHNS/O analyzer. Infrared spectra were recorded with KBr disks on a Shimadzu FT-IR 8300. Nuclear magnetic resonance (NMR) data were obtained using a JEOL eclipse 400+ spectrometer and deuterated dimethylsulfoxide (d6-DMSO) as solvent. The electrical conductivity of a $1x10^{-3}$ $mol.dm^{-3}$ solution of each complex was measured with a Biocristal conductometer, in MeCN. Melting points (MP) were measured on a Microquimica MQAPF-301 apparatus. Full scan mass spectra (MS mode) were obtained on a MicroTOF LC Bruker Daltonics spectrometer equipped with an electrospray source operating in positive ion mode. Samples were dissolved in a MeOH/H_2O (1:1) solution and injected in the apparatus by direct infusion. To prepare the samples for transmission electron microscopy (TEM) the cells were cultured until reaching their final exponential and initial stationary phases. Pellets of cells were then harvested and processed for transmission electron microscopy (TEM) according to routine procedures

as follows: the control and cells treated with the coordination compounds were fixed in 2.5% glutaraldehyde, 4% paraformaldehyde diluited in 0.1 mol L^{-1} cacodilic buffer (pH = 7.2) and post-fixed in 1% osmium tetroxide and 0.8% potassium ferrocyanide, at room temperature, in the dark for 20 minutes. After the fixing step, the dehydration process was conducted with 30, 50, 70, 80, 95 and 100% of acetone and samples were embedded in a crescent series of epoxy resin (Polybed 812®, EUA). Small blocks of the obtained polymer were cut with an ultramicrotome (Reichert Ultracut's, Leica® Switzerland). Ultrathin sections were then negatively stained with uranyl acetate (5%) and lead citrate for observation in the microscopy (TEM 900 Zeiss, Germany), at 80 kV.

2.2 Syntheses

2.2.1 Synthesis of the ligands

The ligands employed in this work are presented in Scheme 1 and were synthesized as described previously [15, 16, 17].

2.2.2. Syntheses and characterizations of the complexes

The syntheses of the zinc complexes followed a similar synthetic route as exemplified below for the synthesis of the compound [Zn(HL1)Cl2] **(1)** (the syntheses and partial characterizations of complexes **(1)** and **(2)** were previously described in the literature [18,19]). Table 1 shows crystallographic data and Table 2 shows some data concerning the synthesis and characterization of the compounds **(1)-(4)**.

[Zn(HL1)Cl_2] **(1):** An isopropanol solution (15 cm^3) of $ZnCl_2.2H_2O$ (136 mg, 1 mmol) was added to a methanol solution (15 cm^3) of the ligand HL1 (200 mg, 1 mmol), resulting in a white solid. The solution was heated (50-60ºC) until complete dissolution of the precipitate. The solution was

refrigerated for some days and white single crystals were formed, filtered off and washed with methanol.

2.3 Crystal data collection and refinement

The molecular structures of the complexes **(1)**, **(2)** and **(3)** were solved by single crystal x-ray diffraction. Crystal data were collected at 295 K from an *Enraf-Nonius Kappa*-CCD diffractometer with graphite monochromatized Mo K_α radiation [20]. The cell parameters were obtained using the *COLLECT*A [21] and *PHICHI* [22] programs, and were refined using the *DIRAX* program [23]. Intensities were corrected by *Lorentz* polarization using the *EvalCCD* program [24], and absorption correction with the *SADABS* program [25]. The structures were solved as described in reference [26]. The positional parameters of the H atoms bonded to C atoms in the methylene moiety were obtained geometrically, with the C-H distances fixed at 0.96Å for Csp^3 atoms, and their respective C atoms were refined with U_{iso}(H) = -1.2Ueq(Csp^3). The positional parameters of the H atoms bonded to C atoms in the aromatic rings were obtained geometrically, with the C-H distances fixed at 0.93Å for Csp^2 atoms, and set to ride on their respective C atoms, with U_{iso}(H) = 1.2Ueq(Csp^2). The hydrogen atoms of the aminic and hydroxyl groups were located in *Fourier maps* and free refined to position. Crystallographic and structure refinement data for complexes **(1)-(3)** are shown in Table 1.

Table 1. Crystallographic data and structure refinement for complexes **(1)**, **(2)** and **(3)**.

Complexes	**(1)**	**(2)**	**(3)**
Empirical formula	$C_{12}H_{13}N_3ZnCl_2$	$C_{13}H_{14}N_2OZnCl_2$	$C_8H_{12}N_2OZnCl_2$
Formula weight	335.52	350.56	288.47
T /K	295(2) K	295(2) K	295(2) K
Radiation, λ/Å	0.71073 Å	0.71073 Å	0.71073 Å
Crystal System, space group	*Monoclinic*, $P2_1/n$	*Triclinic*, *P*-1	*Monoclinic*, $P2_1/c$

Unit cell dimensions in (Å) and (°)	a = 8.4981(17) b = 11.914(2) c = 14.405(3) β = 105.74(3)	a = 8.3502(17) b = 9.4156(19) c = 11.005(2) α = 99.79(3) β = 111.48(3) γ = 108.24(3)	a = 10.131(2) b = 8.0967(16) c = 14.367(3) β = 108.99(3)
Volume /Å^3	1403.8(5)	723.9(3)	1114.3(4
Z	4	2	4
Calculated density/g.cm^{-3}	1.588	1.608	1.720
Absorption coefficient /mm^{-1}	2.114	2.057	2.652
F(000)	680	356	584
Crystal size / mm^3	0.17 x 0.12 x 0.10	0.76 x 0.47 x 0.27	0.22 x 0.21 x 0.15
Theta range /°	3.05 to 25.49	2.10 to 25.50	3.29 to 25.00
Reflections collected	29432	20491	19363
Independent reflections	2614[$R_{(int)}$=0.0726]	2667[$R_{(int)}$=0.0520]	1954 [$R_{(int)}$ = 0.0406]
Completeness to θ max.	99.8 %	99.1 %	99.6 %
Max. and min. transmission	0.8148 and 0.7204	0.6066 and 0.3039	0.6981 and 0.5931
Data / restraints / parameters	2614 / 0 / 167	2667 / 0 / 181	1954 / 0 / 136
Goodness-of-fit on F^2	1.043	1.123	1.041
Final Rindices [I>2sigma(I)]	R_1 = 0.0272 wR_2 = 0.0490	R_1 = 0.032 wR_2 = 0.0681	R_1 = 0.0199 wR_2 = 0.0425
R indices (all data)	R_1 = 0.0478 wR_2 = 0.0531	R_1 = 0.0550 wR_2 = 0.0809	R_1 = 0.0258 wR_2 = 0.0440
Extinction coefficient	None	0.0174(18)	0.0009(3)
Largest diff. peak and hole (e$^-$.Å^{-3})	0.232 and -0.220	0.487 and -0.628	0.271 and -0.238

2.4.Antileukemic activity studies

2.4.1. Culture media

Human leukemia cell lines THP-1 (acute monocytic), U937 (histiocytic lymphoma) and Molt-4 (acute lymphoblastic) were cultured routinely in DMEM-F12 medium (Gibco, BRL), supplemented with 10% fetal calf serum and gentamicin (20 µg/ml; Gibco, BRL) at 37 °C in a humidified atmosphere containing 5% CO_2. Culture media were changed every 2–3 days. Blood samples were collected from healthy donors in Sodium Heparin glass tubes "VacutainerTM" (*Becton Dikinson*). Peripherical blood

mononuclear cells (PBMC) were isolated over Ficoll-Paque™ Plus (1.08 g/mL) in a 50 mL conical tube (2:1 - blood:ficoll). Twenty milliliters of a fresh, heparinized blood sample were diluted in phosphate-buffered saline (PBS), gently laid over 10 ml of Ficoll and centrifuged at 500xg for 20 min at 25 °C. PBMC rings were collected from the interface of blood samples and washed three times with PBS (phosphate buffered saline) by centrifugation at 500xg for 10 min at 4 °C. The supernatant was discarded and the cells were suspended in DMEM-F12 medium (Gibco, BRL). Trypan blue solution 0.4% (Sigma, Germany) was used to count the cells into an appropriate concentration and the viability of cells was checked; the required range of cell viability was 95-99%.

2.4.1. Screening for antileukemic activity

In order to evaluate the *in vitro* antitumoral activity of complexes **(1-4)**, their respective ligands and metallic salt were dissolved in DMSO and tested using THP-1, U937 and Molt-4 cells lines. Cisplatin and DMSO were used, respectively, as a positive and negative control of the assay. To determine cell viability the colorimetric MTT (3-(4,5-dimethylthiazol-2-yl)-2,5-diphenyl tetrazolium bromide) metabolic activity assay was used and IC_{50} values were calculated in order to evaluate the relationship between the structure and the activity of these synthetic compounds (IC_{50} is the concentration required for 50% of inhibition). The MTT assay assesses the capacity of the mitochondrial enzyme succinate dehydrogenase to transform the MTT salt into a purple colored product (formazan), which is proportional to the number of viable cells [27]. Leukemia cells (1×10^6 cells mL^{-1}) in DMEM-F12 medium supplemented with 10% fetal calf serum and 20 μg mL^{-1} gentamicin were plated (100 μL/ well) in 96 well plates and treated with different concentrations of complexes (**1-4**) for 36 h and incubated at 37°C with 5% of CO_2 and humidified atmosphere. Twenty microliters of MTT working solution (5 mg mL^{-1}) were added into each well, and the cells were incubated at 37 °C for 4 h. Then, the MTT-formazan crystals produced by viable cells were dissolved in

an isopropanol-HCl solution. The optical density (OD) values were measured by spectrophotometry at 570 nm using a Microplate Reader (Multiskan-EX). The OD values are presented as relative viable cell numbers. For apoptosis analysis by Annexin V-FITC Apoptosis Detection kit (Sigma®) U-937 cells were seeded in 24-well plates at a density of 1 x 10^6 cells.mL^{-1} and treated with compound **(4)** at concentrations of 200 and 400 µmol L^{-1} and incubated at 37 ºC for 24 h in a humidified atmosphere with 5% CO_2. After 24 h the cells were collected and washed in DPBS and suspended in binding buffer containing 5 µL of annexin V – FITC and 10 µL of propidium iodide. The cells were incubated for exactly 10 minutes (protected from light) at room temperature, according to the manufacturer's recommendations. Data acquisition was performed by BD FACSCalibur with CELLQuest software and for data analysis, WinMDI software version 2.9 was used. For analysis of cell viability and apoptosis the mean and standard error were calculated from the raw data and then subjected to the One-way ANOVA- Turkey´s Multiple Comparison Test (for $ZnCl_2$ and cisplatin) and two-way ANOVA-Bonferroni posttests (for all the complexes, ligands and metallic salt), software Graphpad version 5.0 (analysis of variance). Significant difference was taken as *$p < 0.05$, ** $p < 0.01$ and *** $p < 0.001$.

2.5. Antibacterial activity studies

2.5.1. Microorganisms

Bacterial strains: *S. aureus* (ATCC10832, ATCC25923, COL) and the clinical *S. aureus* LSA88 isolate (SEC/SEF/TSST-1+) were obtained from the bacterial collection of the Laboratory of Animal Health (Laboratorio de Sanidade Animal- LSA), Universidade Estadual do Norte Fluminense Darcy Ribeiro, RJ/ Brazil.

2.5.2 Growth inhibition

The inhibition assay was conducted by adding bacterial cells to grow in BHI (Brain Heart Infusion

Broth) medium during 24 h at 37 ºC. An aliquot of 0.1 mL of innoculum containing 10^8 cells/mL (0.5 McFarland, Densimat (bioMérieux, France) was added to 1.85 mL of medium and 0.5 mL of each compound (ligands, coordination compounds and $ZnCl_2$ at concentration of 10^{-2} mol L^{-1}). As positive and negative controls, gentamicin at concentration of 10^{-2} mol L^{-1} and DMSO were used, respectively. The growth curves were measured with a densitometer $D.O._{550nm}$ (Densimat - bioMérieux, France) in intervals of 60 min. The assays were stopped when cell density reached 7.5 McFarland. Each experiment was performed in triplicates and repeated twice. Inhibition percentages were thus reported as averaged values.

2.5.3 Minimal Inhibitory Concentration (MIC)

In vitro antibacterial activity of the complexes was investigated by the broth microdilution method according to the Clinical and Laboratory Standards Institute (CLSI 2009) document M7-A8 [28]. Mueller Hinton broth (Acumedia, USA), supplemented with 2% glucose, was employed as the bacterial growth medium. Stock solutions of the compounds were prepared in DMSO and diluted in the same culture medium in serial, twofold concentrations in the range of $1.25x10^{-4}$–10^{-3} mol L^{-1}. Through photometric readings (Densimat - bioMérrieux, France) the inoculum containing $1x10^8$ CFU mL^{-1} corresponding to 0.5 McFarland, were obtained from the broth cultures in the log phase of growth and diluted to $1x10^6$ CFU mL^{-1}. Subsequently, a 96 wells cell culture plate (TPP, USA) was used for MIC assays, and serial diluted chemical compound solutions (0.1 mL), inoculated in each sample of each bacterium strain (0.1mL), were incubated in a humid chamber at 37 ºC for 24 h. The MIC of each tested compound was defined as the lowest concentration exhibiting no visible growth compared to the drug-free control wells seen after the addition of 30 µL (1 mg/mL) of the dye resazurin (Sigma, USA). Gentamicin (Sigma, USA) was used as a reference antibacterial agent. A column of plate wells containing only inoculated medium was kept as the negative control. Metallic salt ($ZnCl_2$) and ligand controls were also conducted simultaneously. All assays were performed in triplicates [28].

3. Results and discussion

In our attempt to generate compounds with effective biological activity (i.e. antitumoral and antibacterial), we focused on Zn(II) complexes with distinct N,O-donor ligands, containing one or two aromatic chelating groups (Scheme 1). We have selected those ligands since they allow us (i) to probe if different bipodal ligands have similar coordination behavior and (ii) to investigate the influence of the ligands' structure on the antibacterial and antitumor activities of these complexes.

While the bipodal ligand HL1 induces a N3 coordination environment on the metal center, the bipodal ligands H2L2, H2L3 and H2L4 may generate a N2O coordination, where the O-donor center is provided by a phenol, a primary alcohol and a secondary alcohol, respectively. Ligands H2L3 and H2L4 are similar, but the ligand H2L4 presents a methyl group, which is absent in ligand H2L3.

The ligands and their respective zinc complexes are very stable in air. They are remarkably soluble in polar aprotic solvents such as DMF, DMSO and MeCN; slightly soluble in ethanol, methanol and chloroform; insoluble in water.

The reactions between the ligands described and $ZnCl_2.2H_2O$ allowed the isolation of crystals for all compounds. It was possible to determine the molecular structure through x-ray diffraction for compounds **(1)-(3)**. Table 2 shows relevant data from the synthesis and characterization of the compounds **(1)-(4)**.The conductivity behavior of complexes in MeCN was examined. The low conductivity values observed for complexes **(1)-(4)** suggest that they are non-electrolyte and indicate that the arrangement observed in solid state is the same in solution.

The data presented in Table 2 indicate that the compounds are pure and that compounds **(1)-(4)** are neutral species. Scheme 1 presents the proposed structures of complexes **(1)-(4)**, based on spectroscopic and structural data.

Scheme 1 here

Table 2. Yield, melting point (M.P.), elemental analysis (C, H, N) and conductivity data for complexes **(1)-(4)**, in MeCN.

Complex	Composition	M.W (g/mol)	Yield (%)	M. P. (^{o}C)	%C (Found/Calcd.)	%H (Found/Calcd.)	%N (Found/Calcd.)	Λ_M ($cm^2\,\Omega^{-1}\,mol^{-1}$)
(1)	$Zn(HL1)Cl_2$	335.54	78	286	42.86/42.96	3.95/3.91	12.56/12.52	5.6
(2)	$Zn(H_2L2)Cl_2$	350.55	79	193	44.57/44.54	4.03/4.03	8.24/7.99	17.3
(3)	$Zn(H_2L3)Cl_2$	288.48	63	169	33.47/33.31	4.21/4.19	9.98/9.71	3.8
(4)	$Zn(H_2L4)Cl_2$	302.51	68	175	35.40/35.73	4.89/4.66	9.16/9.26	16.8

3.1. IR and NMR spectra

The IR spectra of complexes **(1)-(4)** were analyzed in comparison with those of their common free ligands HL_1-H_2L_4 in the region 4000-400 cm^{-1}. The IR spectra of free ligands are similar and show characteristic absorption bands: ν_{N-H} ,$\nu_{C=C}$, $\nu_{C=N}$ and $\delta_{(pyridine\ ring)}$. For ligand HL1, characteristic bands of the pyridine group are observed at 1593, 1435 and 758 cm^{-1}, assigned to $\nu_{C=N}$, $\nu_{C=C}$ and $\delta_{(pyridine\ ring)}$, respectively. The ν_{N-H} band is observed at 3344 cm^{-1} for ligand HL1. For ligand H2L2, characteristic bands of the pyridine group are observed at 1593, 1430 and 756 cm^{-1}, assigned to $\nu_{C=N}$, $\nu_{C=C}$ and $\delta_{(pyridine\ ring)}$, respectively. The ν_{N-H} band is observed at 3263 cm^{-1}. There is a band at 1280 cm^{-1}, attributed to the phenol group (νC-O). For ligand HL3, characteristic bands of the pyridine group are observed at 1595, 1435 and 762 cm^{-1}, assigned to $\nu_{C=N}$, $\nu_{C=C}$ and $\delta_{(pyridine\ ring)}$, respectively. The ν_{N-H} band is observed at 3300 cm^{-1}. For ligand H2L4, characteristic bands of the pyridine group are observed at 1595, 1437 and 764 cm^{-1}, assigned to $\nu_{C=N}$, $\nu_{C=C}$ and $\delta_{(pyridine\ ring)}$, respectively. The ν_{N-H} band is observed at 3300 cm^{-1}. For all the complexes, the bands due to ν_{N-H} and $\delta_{(pyridine\ ring)}$ exhibited downward and upward shifts, respectively, after coordination to $ZnCl_2$. For complexes **(1)-(4)**, the ν_{N-H} are observed at 3244, 3226, 3228 and 3178 cm^{-1}, and $\delta_{(pyridine\ ring)}$ are observed at 760, 760,779 and 767 cm^{-1}, respectively. The bands attributed to $\nu_{C=N}$ exhibited a downward shift, resulting in bands at 1570, 1570 and 1573 cm^{-1}, respectively for complexes **(1), (3)** and **(4)**. For complex **(2)**, no shift was observed for the band $\nu_{C=N}$; furthermore, the presence of a band at 1273 cm^{-1} indicates the presence of

the phenol group in the structure of the complex, in good agreement with the crystal data. Table 3 presents the characteristic bands of L1-L4 and their respective complexes.

Table 3. The characteristic IR bands of the ligands L1-L4 and their respective complexes, in cm^{-1}.

	HL1	(1)	H2L2	(2)	H2L3	(3)	H2L4	(4)
ν_{N-H}	3344	3244	3263	3226	3300	3228	3300	3178
$\nu_{C=N}$,	1593	1570	1593	1593	1595	1570	1595	1573
$\nu_{C=C}$	1435	1442	1430	1435	1435	1446	1437	1442
$\delta_{(pyridine\ ring)}$	758	760	756	760	762	779	764	767
phenol (νC-O)	---		1280		----		---	1273

The ^{1}H NMR spectra for the complexes are presented in Figure 1. To facilitate the interpretation, the carbon atoms in the ligands are numbered, and the numbers on the signals indicate the hydrogen atom attached to these carbon atoms. The spectra for complexes **(1)**, **(3)** and **(4)** show a similar profile related to the aromatic region (7.0-9.0 ppm), which is attributed to the hydrogen atoms of the pyridine group. Interestingly, while these complexes show only three signals related to these aromatic hydrogen atoms, their free ligands display four signals (see Table 4). The integral ratio and the coupling constant indicate that the signals of the hydrogen atoms bound to the carbon atoms 2 and 4 were merged in a multiplet around 7.56 ppm.

For complex **(1)** the methylenic hydrogen (CH_2) from the ligand HL1 is observed at 4.13 ppm with a very broad shape, while in the free ligand it appears as a narrow singlet at 3.90 ppm. For the same complex, the amine hydrogen atom was observed at 2.90 ppm in the free ligand and appears at 4.93 ppm in the complex. This shift is in agreement with the fact that the electron density on the nitrogen atom is lower in the complex than in the free ligand.

The spectrum of complex **(3)** shows the methylenic group attached to the aromatic ring as a singlet at 4.06 ppm (3.92 ppm in the free ligand). There are also two triplets (J = 5.5 Hz) associated with the other two methylenic groups, at 3.51 and 2.78 ppm. The former is the one bound to the alcohol group while the latter is connected to the amine nitrogen atom.

For complex **(4)**, the hydrogen atoms from the py-CH_2-N unit were split in two doublets with J values of 15.6 Hz, typical of geminal hydrogen atoms. The hydrogen atom bound to C8 appears at 3.74 ppm as a broad singlet, while the hydrogen atoms from the methylenic and methyl groups are observed at 2.77 ppm (dd, J_1 = 11.8 Hz; J_2= 3.13 Hz) and 1.07 ppm (d, J = 6.3 Hz), respectively.

The spectrum of complex **(2)** differs significantly from the others, since it possesses two different aromatic rings (pyridine and phenol), resulting in a larger number of signals in the ^{1}H NMR spectrum between 6 and 9 ppm. The assignment of the hydrogen atoms from the pyridinic group may be established by comparison to the compounds described above. However, it should be pointed out that some of the aromatic hydrogen atoms are presenting two different signals, accounting to a ratio of 20-30/70-80 %. For example, the hydrogen atom attached to C1 presents just one signal in compounds **(1), (3)** and **(4)**. However, in **(2)** there are two signals associated with this hydrogen atom (8.75 ppm, d, J = 4.0 Hz and 8.59 ppm, d, J = 3.1 Hz). Similarly, there are other signals in the aromatic range which present the same ratio and are associated with the same hydrogen atoms (C3-H, C4-H, C11-H). On the other hand, there are some signals that are not split (C2-H, C9-H, C10-H, C12-H). We have already observed the same behavior with another zinc compound synthesized with a ligand which also contains pyridine and phenol groups; those studies seem to indicate the presence of different isomers in solution [9]. The aliphatic region is dominated by two intense broad signals at 3.95 ppm and 4.08 ppm, which are associated with the methylenic hydrogen atoms. There are also some side peaks that again suggest the presence of different isomers in solution. In the free ligand the methylenic hydrogen atoms appear at 4.00 and 3.83 ppm. Table 4 shows the relevant ^{1}H NMR spectral data with assignments.

Table 4. ^{1}H NMR spectral data with assignments for ligands HL1-H2L4 and their respective complexes.

H	L1	ZnL1 (1)	L2	ZnL2 (2)	L3	ZnL3 (3)	L4	ZnL4 (4)
	δ/M/*J* (*Hz*)	δ/M/*J* (*Hz*)	δ/M/*J* (*Hz*)	δ/M/*J* (*Hz*)	δ/M/*J* (*Hz*)	δ/M/*J* (*Hz*)	δ/M/*J* (*Hz*)	δ/M/*J* (*Hz*)
1	8.48/dd/ 4.0; 1.8	8.78/d/4.7	8.58/dd/5.3; 1.7	8.76/d/4.0 8.59/d/3.1	8.47/d/4.2	8.56/d/5.08	8.54/d/4.2	8.55/d/4.7
2	7.07/m	7.55/m	7.19/m	7.50/m	7.11/dd/7.7; 4.4	7.55/m	7.15/dd/7.7; 4.8	7.53/m
3	7.56/dt/7.7; 1.8	8.02/dt/7.6; 1.6	7.65/dt/7.7; 1.7	7.96/t/7.6 7.70/dt/7.8; 1.6	7.59/dt/7.7; 1.5	8.03/dt/8.0; 1.5	7.63/dt/7.7; 1.8	8.01/dt/7.8; 1.2
4	7.28/d/7.7	7.55/m	7.19/m	7.50/m 7.08/d/7.4	7.23/d/7.7	7.55/m	7,26/d/7.7	7.53/m
6	3.90/s	4.13/s	3.83/s	3.95/s	3.87/s	4.06/s	3.91/s	4.06/d/15.6 3.98/d/15.6
7	-	-	4.0/s	4.08/s	-	-	-	-
9	-	-	6.97/d/7.3	7.25/d/6.6	-	-	-	-
10	-	-	6.77/dt/7.3; 0.9	6.78/t/7.4	-	-	-	-
11	-	-	7.19/m	6.36/t/7.0 7.17/t/7.6	-	-	-	-
12	-	-	6.86/m	6.86/d//6,9 6,89/d/6,9	-	-	-	-
13	-	-	-	-	2.76/t/5.3	2.78/t/5.5	2.74/dd/12.9; 2.2 2.41/dd/12.9; 9.5	2.76/dd/12.0; 3.1
14	-	-	-	-	3.61/t/5.3	3.51/t/5.5	3.81/m	3.73/ m
15	-	-	-	-	-	-	1.13/d/6.2	1.06/d/6.2

δ= chemical shift; M = signal multiplicity, *J* = *coupling constant.*

3.2. Structure of the complexes

*3.2.1. Description of the structure of complexes **(1)-(3)***

The single crystal x-ray studies are in agreement with the above spectroscopic analysis and show three new structures of mononuclear zinc complexes with σ-N_3(HL1), σ-N_2(H2L2) andσ-N_2O_1 (H2L3) donor sets. The *ORTEP*-3 projection of **(1)**, **(2)** and **(3)** are shown in Figures 2-4, respectively. Bond lengths and bond angles are listed in Table 5. These parameters are in agreement with literature values [29] and within the expected range for compounds of this class, as presented by the *International Tables for X-ray Crystallography* [30].

Table 5. Selected bond lengths [Å] and angles [°] for complexes **(1)**, **(2)** and **(3)**.

Bond lengths	**(1)**	**(2)**	**(3)**
Zn1-N1	2.1548(19)	2.031(2)	2.1244(16)
Zn1-N2	2.146(2)	2.057(3)	2.0971(17)
Zn1-N3	2.158(2)	-----	-----
Zn1-O1	-----	-----	2.3150(17)
Zn-Cl1	2.2650(7)	2.1988(10)	2.2180(7)
Zn-Cl2	2.2598(7)	2.2214(13)	2.2679(7)
N2-C6	1.453(3)	1.475(4)	1.463(2)
N2-C7	1.461(3)	1.475(4)	1.463(3)
N1-C5	1.332(3)	1.343(4)	1.334(2)
N1-C1	1.335(3)	1.315(4)	1.327(3)
O1-C8	-----	-----	1.410(3)
O1-C9	-----	1.337(4)	-----
Bond angles	**(1)**	**(2)**	**(3)**
C6-N2-C7	115.7(2)	113.7(2)	114.22(16)
N2-Zn1-N1	76.00(7)	81.66(10)	77.95(6)
N2-Zn1-N3	76.44(8)	-----	-----

N1-Zn1-N3	150.22(8)	-----	-----
N2-Zn1-Cl2	139.63(6)	113.74(9)	124.64(5)
N1-Zn1-Cl2	96.53(5)	109.13(8)	98.30(5)
N3-Zn1-Cl2	97.16(6)	-----	-----
N2-Zn1-Cl1	103.56(6)	112.38(8)	115.11(5)
N1-Zn1-Cl1	97.76(6)	116.17(8)	103.69(5)
N3-Zn1-Cl1	99.43(6)	-----	-----
Cl2-Zn1-Cl1	116.80(4)	118.25(4)	119.26(2)
N2-Zn1-O1	-----	-----	74.00(6)
N1-Zn1-O1	-----	-----	151.08(6)
Cl1-Zn1-O1	-----	-----	94.51(5)
Cl2-Zn1-O1	-----	-----	91.94(5)

Incomplete structural data for complex **(1)** were previously reported in 1992 [31]. In 2007, Kang and co-workers reported the structural data for the complex $[ZnCl_2(HL1)].CHCl_3$, revealing the presence of a chloroform as solvate in the molecular structure [32]. Here, we are reporting the structural data for complex **(1)** without solvate molecule (Figure 2). In **(1)**, the zinc center is coordinated by a σ-N_3 donor set provided by the ligand HL1, *via* one aminic nitrogen atom (N2H), two pyridinic nitrogen atoms (N1 and N3) and two chloride anions (Cl1 and Cl2), resulting in a pentacoordinated zinc(II) complex with a N3Cl2 coordination environment around the zinc(II) center. The tridentate ligand HL1 is linked to the zinc(II) ion by two five-membered rings, with the following bite angles: 76.00(7°) from N1-Zn-N3 and 76.44(8°) from N2-Zn-N3. In this complex the τ parameter ($\tau = (\beta-\alpha)/60 = 0.18$) indicates a slightly distorted square pyramidal geometry [33]. The basal positions are occupied by N1, N2, N3 and Cl2, while the axial position is occupied by Cl1 atom. The base of the pyramid shows the following angles: β = 150.22(8)° from N1-Zn1-N3 and α = 139.63(6)° from N2-Zn1-Cl2. The zinc center shows a dihedral angle with N1/C5/C6/N2 plane of 30.4(1)° and a

torsion angle for this fragment (N1-C5-C6-N2) of -24.2(3)°. The zinc atom shows a deviation of 0.594 Å out of the N1/N2/N3/Cl2 plane.

Although it has been shown that the ligand H2L2 usually provides a N2O1 donor set, when reacted with to $ZnCl_2.2H_2O$ [34, 16, 35], it acts as a bidentate ligand through the aminic (N2) and the pyridinic nitrogen (N1) atoms (Figure 3). The distorted tetrahedral geometry presented by the zinc center is completed by two chloro ligands. The angles around the zinc center are 81.7(1)° for N1-Zn1-N2 and 118.26(4)° for Cl1-Zn1-Cl2. The phenol group remains protonated after coordination and away from the metal center, indicating that the hydrogen bonds of the O1H from the phenolate group with H6B (from C6) and H7B (from C7) are strong. This behavior is different from what we observed previously in the compound [Zn^{II}(HBPClNOL)Cl], in which the phenol group is coordinated to the zinc center as an anion [12]. This suggests that the Zn(II) ion in **(2)** has a lower acidity than in the complex [Zn^{II}(HBPClNOL)Cl]. The structure for complex (2) is in excellent agreement with that proposed by Tandon and co-workers in 1994 [19].The molecular structure of the complex **(3)** reveals a pentacoordinated zinc center (Figure 4), which adopts a strongly distorted square pyramidal geometry ($\tau = 0.44$). The basal positions are occupied by N1, N2, O1 and Cl2 atoms, and the axial position is occupied by the Cl1 anion. The basal angles are β = 151.08° for N1-Zn1-O1 and α = 124.64° for N2-Zn1-Cl2. Although the ligand H2L3 is very similar to H2L2, also providing a N2O donor set, it is able to act as a tridentate ligand, while the latter showed a bidentate coordination behavior. Thus, the Zn(II) ion coordinates to the H2L3 ligand *via* the pyridinic nitrogen atom (N2), aminic nitrogen atom (N1) and by the alcohol group (O1H). Two chloride anions (Cl1 and Cl2) are also bound to the Zn(II) center, resulting in a N_2OCl_2 coordination environment. The two five-membered rings observed in the complex have bite angles of 77.95(6)° in N2-Zn1-

N1 and 74.00(6)° for N2-Zn1-O1, which are very similar to those observed in complex **(1)**. The zinc atom shows a deviation of 0.715 Å out of the N1/N2/O1/Cl2 equatorial plane. The metal atom forms a dihedral angle with the N1/C5/C6/N2 plane of 27.2(1)° and an N1-C5-C6-N2 torsion angle of -31.6(2)°. The dihedral angle formed by N2/C7/C8/O1 is 17.1(1)° and the torsion angle in this N2-C7-C8-O1 moiety is 52.43(2)°.

3.3. ESI(+)-MS and ESI(+)-MS/MS studies

For complex **(1)**, in a water/methanol solution (1:1), signals associated with mononuclear and dinuclear species are observed ($[Zn(NaL1)Cl]^+$ (*m/z* 322) and $[(HL1)(OH_2)(OH)Zn\text{-}(\mu\text{-}Cl)\text{-}Zn(HL1)(OH)(H_2O)]^+$ (*m/z* 635)), as well as signals related to the free ligand $[H2L1]^+$ (*m/z* 200). The observation of the *m/z* 635 species in the MS/MS spectrum suggests the formation of the mononuclear cation $[Zn(HL1)(OH)(OH_2)]^+$ (*m/z* 300), by the loss of the neutral molecule $[Zn(HL1)(Cl)(OH)(OH_2)]$ (*m/z* 335).

As complex **(2)** is neutral, *i.e.* $[Zn(HL2)Cl_2]$, no signal associated with this species is observed. However, in a water/methanol (1:1) solution, twelve additional signals and their characteristic set of iso-topolog ions, due mainly to the presence of Zn and Cl atoms, are clearly detectable (data not shown). These signals are related to mono- and dinuclear species containing Zn, *e.g*: $[Zn(HL2)]^+$ (*m/z* 277), $[Zn(H2L2)Cl]^+$ (*m/z* 313), $[Zn(NaHL2)Cl]^+$ (*m/z* 335), $[Zn(NaH2L2)(OH)(Cl)(CH_3OH)]^+$ (*m/z* 385), $[Zn(H2L2)(HL2)]^+$ (*m/z* 493), $[Zn(H2L2)(HL2)(CH_3OH)_2]^+$ (*m/z* 555), $[(HL2)Zn\text{-}(\mu\text{-}OH)\text{-}Zn(HL2)]^+$ (*m/z* 571), $[(HL2)Zn\text{-}(\mu\text{-}Cl)\text{-}Zn(HL2)]^+$ (*m/z* 589) and $[(NaHL2)Zn\text{-}(\mu\text{-}Cl)\text{-}Zn(HL2)Cl]^+$ (*m/z* 647). In addition, a signal attributable to the ligand H2L2 (*i.e.* $[H3L2]^+$ (*m/z* 215)) is observed. MS/MS studies indicate that the ion of *m/z* 533 may

yield the cation $[Zn(H2L2)(HL2)]^+$ (*m/z* 493) by the loss of solvent, suggesting that the *m/z* 533 species is probably a solvent cluster of the $[Zn(H2L2)(HL2)]^+$ (*m/z* 493) ion. MS/MS analysis of the species with *m/z* 493 yields the cation $[Zn(HL2)]^+$ (*m/z* 279) and the neutral molecule of the ligand H2L2 (*m/z* 214). The ion corresponding to *m/z* 482 may be associated with dimerization of the H2L2 ligand and solvent molecules. MS/MS data of the ion with *m/z* 482 indicates the formation of C_7H_6O (*m/z* 106), as reported previously [24]. In water/methanol solutions interesting association processes are observed rendering the species $[(HL2)Zn-(\mu-OH)-Zn(HL2)]^+$ (*m/z* 571), $[(HL2)Zn-(\mu-Cl)-Zn(HL2)]^+$ (*m/z* 589) and $[(NaHL2)Zn-(\mu-Cl)-Zn(HL2)]^+$ (*m/z* 647) as a result of the interaction between the two $[Zn(HL2)]^+$ *m/z* 277 ions. The ion with *m/z* 571 is formed by the interaction between two species of *m/z* 277 *via* a hydroxo bridge; the ion with *m/z* 589 is formed by an interaction between two species with *m/z* 277 involving a chloride bridge and for the ion with *m/z* 647it is suggested that it may contain the species with *m/z* 589 plus a chloride and a sodium ion. ESI(+)-MS/MS of these ions were unsuccessful due the low intensity of the majority of the signals. ESI(+)-MS/MS for the species with *m/z* 277, 482 and 491 are also structurally characteristic, indicating only the presence of the ligand H2L2 in these fragments.

ESI(+)-MS data for complex **(3)** indicate the presence of five cations in water/methanol (1:1) solution: $[H3L3]^+$ (*m/z* 153), $[Zn(HL3)]^+$ (*m/z* 215), $[Zn(H2L3)2(Cl)]^+$ (*m/z* 403), $[(HL3)Zn-(\mu-Cl)-Zn(H2L3)Cl]^+$ (*m/z* 505) and $[(H2L3)(Cl)Zn-(\mu-Cl)-Zn(H2L3)(Cl)]^+$ (*m/z* 541). The ESI(+)-MS/MS of the ion with *m/z* 541 is also structurally characteristic; the ion loses an HCl molecule to form a fragment ion with *m/z* 505 $[Zn_2(HL3)(H2L3)Cl_2]^+$. The loss of two HCl molecules leads to the formation of the fragment ion with *m/z* 469, $[Zn_2(HL3)_2Cl]^+$. The loss of the neutral complex $[Zn(H2L3)Cl_2]$ (*m/z* 288) results in a fragment ion with *m/z* 253

$[Zn(H2L3)Cl]^+$.

For complex **(4)** five species were detected in the ESI(+)-MS spectrum: $[NaH2L4]^+$ (*m/z* 189), $[NaZn(HL4)Cl)]^+$ (*m/z* 287), $[Zn(H2L4)(HL4)]^+$ (*m/z* 395), $[NaZn_2(L4)_2]^+$ (*m/z* 480) and $[Zn_2(HL4)_2Cl]^+$ (*m/z* 495). The ESI(+)-MS/MS data for these species indicate the presence of the ligand H2L4. Figure 5 illustrates some species detected in the ESI(+)-MS and ESI(+)-MS/MS spectra for compounds **(2)** and **(4)** in H_2O/MeOH. Based on the ESI(+)-MS and ESI(+)-MS/MS data, it is suggested that complex **(4)** is mononuclear in the solid state, with the zinc center coordinating to one molecule of the H2L4 ligand and to chloride ions, thus resulting in a neutral complex, in good agreement with other results (*i.e.* conductivity measurements, NMR and elemental analysis, see above). In solution it can however dimerize, as observed for the other compounds.

The spectra and the proposed structures based on the isotopic pattern for the main ion of each complex are supplied in the Supplementary material.

3.4. Antileukemic activity of the complexes

In order to study the antitumoral activity of the zinc complexes **(1)-(4)**, their cytotoxicity against THP-1, U937 and Molt-4 human leukemia cell lines was investigated (Table 6). Complex **(4)** has a lower IC_{50} value (75 ± 1 μmol L^{-1}) for the U937 cell line, and is the complex with the highest activity of this series. Ligand HL1 is the only ligand with measurable antitumoral activity in the three cell lines under investigation, with an IC_{50} value of 52 ± 1 μmol L^{-1} in the Molt-4 cell line. No potentiating effect is observed upon coordination of HL1 to $ZnCl_2$ since complex **(1)** exhibits very low activity against U937 and Molt-4 and moderate activity against THP-1 cell lines (116 ± 1 μmol L^{-1}). Based on their IC50 values, the zinc complexes are only

weakly active, at best over an order of magnitude less potent than cisplatin.

Table 6. The 50% inhibitory concentration (IC_{50}) of the zinc complexes described in this study and their respective ligands, as well as DMSO and cisplatin, for leukemia cancer cell lines (THP-1, U937 and Molt-4).

Compound	IC_{50} (μmol L^{-1})		
	THP-1	U937	Molt-4
HL1	118.5 ± 10.5	141 ± 1	55 ± 3
(1)	103.5 ± 12.5	> 400	> 400
H2L2	> 400	> 400	> 400
(2)	107 ± 19	> 400	> 400
H2L3	> 400	> 400	> 400
(3)	108.5 ± 6.5	122 ±1	210 ± 8
H2L4	> 400	> 400	> 400
(4)	98.5 ± 8.5	75 ± 1	235.5 ± 5.5
Cisplatin	9.5 ± 1.5	7.5 ± 0.5	6 ± 1
$ZnCl_2$	302 ± 8	123± 13	137 ± 1

The cytotoxicity of the complexes was determined after 36 h of incubation, using the MTT method [27]. * Data represent the mean of a triplicate experiment which was repeated twice.

Based on the moderate activity of complex **(4)** in the U937 cell line, we decided to investigate the mechanism of cell death promoted by this complex. For this purpose, the Annexin V-FITC/PI staining assay was employed. In this assay, U937 cells stained single-positive for Annexin V-FITC are considered mostly early apoptotic cells and cells stained single-positive for PI are predominantly necrotic cells. Cells that are stained

double-positive are considered as late apoptotic or secondary necrotic cells [36]. The Annexin V-FITC/PI staining data indicate that the percentage of apoptosis was 90.8% and 99.1%, respectively, after treatment for 24h with 200 and 400 μmol L^{-1} **(4)**, respectively (see Figure 6c and 6d). For comparison, Figure 6a presents the results for a control group and Figure 6b those collected in presence of cisplatin. For cisplatin, the apoptosis and necrosis rates are 41 % and 16 %, respectively, while the normal cells reaches 44%, at a concentration of 50 μmol L^{-1} after 24h of incubation. These data strongly suggest that complex **(4)** could effectively induce apoptosis in U937 cells in a concentration-dependent manner. It is worth noting that apoptosis is a desired pathway for cell death to occur when developing anticancer agents since apoptosis or programmed cell death is central to the development of homeostasis of metazoans [37].

3.5. Transmission Electron Microscopy

*3.5. 1.Morphological changes of the leukemia cell line U937 after treatment with complex **(4)***

In order to directly observe the morphological changes of the internal structure of human leukemia cells (THP-1 and U937) after the treatment with complex **(4)**, transmission electron microscopy (TEM) was employed.

After incubation times, which varied from 6 h to 12 h, samples were collected to measure cell density and morphological changes. The concentration of complex **(4)** was also varied (100 and 200 μmol L^{-1}, respectively) to assess its effect on the cells.

Figure 7 shows the morphological changes promoted by complex **(4)**, at a concentration of 100 μmol.L^{-1} after 6 h of incubation. A clear association between mitochondria (M) and endoplasmic reticulum (ER) was observed, indicating the initiation of apoptosis. At a concentration of 200 μmol. L^{-1} and after 12 h of incubation

(Figure 8), an intense vacuolization of the cells, condensation of the nuclear chromatin (NC) and the formation of vacuoles (V) were clearly observed. Figure 8 also demonstrates the intense association between mitochondria (M) and the endoplasmic reticulum (ER), as well as the formation of membrane blebs (B). Blebs are typical of apoptotic cells, indicating that complex **(4)** is promoting cell death *via* an apoptotic mechanism.

*3.5.2. Morphological changes of the leukemia cell line THP-1 after treatment with complex **(4)***

THP-1 cells were treated similarly (6-12 h incubations at complex concentrations of 100 and 200 μmol L^{-1}). An increased association between mitochondria (M) and the endoplasmic reticulum (ER) was also observed, as well as a large number of structurally altered mitochondria and large vacuoles with membranous structures, shown in Figures 9 and 10, respectively. In Figure 9, ER-like elements in close proximity to highly altered mitochondria (M) appear with an empty matrix (star), displaying only cristae structures, or possibly extruding their content, resulting in the formation of a vacuole (arrow). Different stages of cell death are observed, leading ultimately to the appearance of abnormal mitochondria (M) and their subsequent destruction, as well as the formation of vacuoles with membranous content (V). Figure 10 shows a multitude of long vacuoles (V) with membranous structures inside (star).

3.6. Antibacterial activity of the complexes

Since we have previously described that the zinc complex [Zn(HBPClNOL)Cl] was very effective on different *S. aureus* strains, we were interested in evaluating if simpler zinc complexes would show similar activity. Table 7 presents the

antibacterial activities of the complexes **(1)-(4)**, of the metallic salt, and of their respective ligands and gentamicin (standard drug), which were evaluated in terms of growth inhibition curves (*i.e.* percentage of inhibition) of *S. aureus* strains (ATCC10832, ATCC25923, COL and LSA88).

Complex **(2)**, at a concentration of 10^{-2} mol L^{-1}, showed the best inhibitory activity reaching 100% of inhibition on each of the four strains under investigation. In contrast, complex **(4)** was the least effective, showing very low inhibitory activity against ATCC25923 (0%), COL (17%) and LSA88 (16%). However, this complex showed high antibacterial activity against ATCC10832 (96%), demonstrating the effect of the coordination of zinc to the ligand, since no activity was observed for the ligand H2L4 alone (see Table 7). The values for the percentage of inhibition of complex **(4)** are very similar to those of its respective ligand H2L4: ATCC25923 (0%), COL (12%) and LSA88 (5%). Ligands H2L3, H2L3 and H2L4 showed low inhibitory activities against this group of tested bacteria (ATCC10832 (5, 0 and 0%, respectively), ATCC25923 (2.4, 0 and 0 %, respectively), COL (11, 12 and 12%, respectively) and LSA88 (6.2, 4 and 5%, respectively)), thus demonstrating that the antibacterial activity of zinc complexes against ATCC10832 is the result of a potentiating effect between the ligands H2L2, H2L3 and H2L4 and zinc(II) ion. For complex **(1)**, high activity was observed only against ATCC10832 (96%). Since complex **(2)** was the most active, experiments to determine its minimum inhibitory concentration (MIC) were carried out against the same strains of *S. aureus*, resulting in values of 512 µg/mL, 512 µg/mL, 512 µg/mL and > 512 µg/mL to ATCC 10832, ATCC 25923, COL and LSA88, respectively (512 µg/mL ≈ 1.46 mmol L^{-1}).

The values obtained for ATCC10832 and ATCC25923 are 32 times higher than those determined with gentamicin, a clinical drug. However, for COL, the MIC was

only twice the value determined for gentamicin. Previously reported MIC values for the complex [Zn(HBPClNOL)Cl], the most active against nine strains of *S. aureus*, are cited, which were all shown to be ~100 times higher than those obtained with chloroamphenicol [12]. As presented in Table 7, complex **(2)** was the most active and its antibacterial activity could be related to the phenol group and to the potentiating effect between the ligand H2L2 and $ZnCl_2$. The same effects were observed for complex [Zn(HBPClNOL)Cl], reported previously [12]. This complex presents a phenol group coordinated to the zinc(II) center and showed the best inhibitory activity, reaching almost 100% of inhibition against nine strains of *S. aureus* under investigation.

Table 7. Antibacterial activities of the complexes **(1)-(4)**, their respective ligands, metallic salt and gentamicin against pathogenic bacteria (*S. aureus*) after 10 h of incubation.

Compound	**% inhibition promoted by the compounds**			
	S. aureus			
	ATCC10832	**ATCC25923**	**COL**	**LSA88**
HL1	8	7	15.3	14.6
(1)	96	51	67	52
H2L2	5	2.4	11	6.2
(2)	100	100	100	100
H2L3	0	0	12	4
(3)	92	15	14	23
H2L4	0	0	12	5
(4)	96	0	17	16
$ZnCl_2$	0	1	5.6	0
Gentamicin	100	100	99	100

*3.6.1. Morphological changes of S. aureus cells after treatment with complexes **(1)** and **(2)***

To directly observe the morphological changes of the internal structure of bacterial cells after the treatment with complexes **(1)** and **(2)**, TEM was employed. Complexes **(1)** and **(2)** were chosen since complex **(1)** exerts strong inhibition and complex **(2)** approximately half that of complex **(1)**. As shown in Figure 11, when *S. aureus* (LSA88) was treated with complex **(1),** the majority of the cells presented debris with small structures resembling cell wall parts; some cells suggested the condensation of DNA (indicated by a star), in agreement with the moderate inhibition promoted by this complex on *S.aureus* cells (see Figure 11B). Figure 11C reveals the formation of membrane-derived vesicles (MVs) (indicated by an arrow), which can be a kind of defense mechanism against the drug, as suggested by Lee and co-workers [38]. According to their study, membrane-derived vesicles (MVs) are produced by Gram-positive bacteria and the subsequent delivery to host cells could be related to the virulence since many virulence-associated proteins were identified in the *S. aureus* MVs. This was the first report describing the importance of MVs as vehicle for delivery of bacterial effector molecules to host cells. Figure 11D reveals the presence of DNA condensation (indicated by a star) and inner walls with aberrant division planes (indicated by arrows) which could be related to the inhibition of wall protein synthesis which, in turn, is directly related to the cellular division process [39]. Figure 12A shows control cells of *S. aureus* with a well defined cell wall and DNA during cell division after 24 h of incubation with complex **(2)**. As shown in Figure 12B, the treatment with complex **(2)** promotes disruption of the cell, with the presence of holes and the extrusion of the cytosolic material. Thus, it is possible to suggest that the high inhibitory activity of complex **(2)** may be associated with the inhibition of the cell division process

of *S.aureus* cells, as an effect of the reduced integrity of *S. aureus* cell wall after treatment with this complex. Due to the presence of groups which resemble amino acids in their structures, complex **(2)** may be working as a host defense peptide (HDPs), defined as important effector molecules of the innate immune system, providing effective barriers against a wide range of invading microorganisms [40]. HDPs interfere with the cell wall biosynthesis machinery and TEM data strongly suggest that they promote local injuries in the cell wall layer leading, as a result of osmotic pressure, to the formation of membrane protrusions with cytoplasmic content [39]. This proposal is in good agreement with transmission electron micrographs, which indicate that the treatment of *S. aureus* with complex **(2)** may lead to lysis after 24 h of incubation.

4. Conclusions

In this work we have described the synthesis and characterization of four zinc complexes containing N,O-ligands. Complexes **(1)**, **(2)** and **(3)** were characterized by x-ray diffraction studies, revealing the presence of mononuclear compounds in the solid state. Complexes **(1-4)** promoted cell death of human leukemia THP-1, U937 and Molt-4 cells *in vitro*. Complex **(4)** exhibited the highest cytotoxic activity with an IC_{50} value of 75 ± 1 μmol L^{-1} against U937, promoting cell death by apoptosis (confirmed by the Annexin V assay). Morphological investigations using TEM analysis revealed an intense association between mitochondria and the endoplasmic reticulum, and the formation of membrane blebs, typical of apoptotic cells, thus indicating that complex **(4)** is promoting cell death by an apoptotic mechanism.

With respect to antibacterial activity, complex **(2)** showed the highest inhibitory activity, reaching almost 100% of inhibition against the three strains under investigation at a concentration of 10^{-2} mol L^{-1}. This result demonstrates that the zinc complexes with

pyridine and phenol ligands are promising lead compounds in the search for new antibacterial drugs. Morphological investigations by TEM indicated that the antibacterial activity of complex **(2)** may be associated with the inhibition of cell wall protein synthesis, which affects cell division.

We are currently carring out additional investigations which aim to shed light into the details of the apoptotic mechanism, as well as to evaluate the activity of complex **(4)** *in vivo* since no modern chemotherapy includes zinc adjuvants, even though zinc serum levels are usually low in leukemic children.

Acknowledgements

A. H. Jr. and C. F. are grateful to financial support received from CAPES (Procad), CNPq (Universal and INCT- Catalise) and FAPERJ (Jovens Cientistas do Nosso Estado, Emergentes). The authors are grateful to LDRX-UFF (Laboratório de Difratometria de Raios-X, Universidade Federal Fluminense) for X-ray facility. Thanks are given to the Consejo Superior de Investigaciones Científicas (CSIC) of Spain for the award of a license for the use of the Cambridge Crystallographic Data Base (CSD). G. S. would like to acknowledge the award of a Future Fellowship (FT120100694) from the Australian Research Council.

Appendix A. Supplementary material

CCDC 852518, 852519 and 852520 contains the supplementary crystallographic data for this paper (complexes **(1)**, **(2)** and **(3)**, respectively). These data can be obtained free of charge from The Cambridge Crystallographic Data Centre via www.ccdc.cam.ac.uk/data_request/cif. Dose-response curves were obtained by MTT

assay and are presented as supplementary material (Figures S1, S2 and S3, respectively for THP-1, U937 and Molt-4 cells).

References

[1] C. T. Chasapis, A. C. Loutsidou, C. A. Spiliopoulou, M. E. Stefanidou, Arch. Toxicol. 86 (2012) 521.

[2] S. Emani, S. J. Hosseinimehr, S. M. Taghdisi, S. Akhlaghpoor, Bioorg. Med. Chem. Let. 17 (2007) 45.

[3] Q. Huang, Z. Pan, P. Wang, Z. Chen, X. Zhang, , H. Xu, Bioorg. Med. Chem. Let. 16 (2006) 3030.

[4] S. Fujimoto, H. Yasui, Y. Yoshikawa, J. Inorg. Biochem. 121 (2013) 10.

[5] M. C. Rodrigues- Argüelles, P. Tourón-Touceda, R. Cao, A. M. García-Deibe, P. Pelegatti, C. Pelizzi, F. J. Zani, J. Inorg. Biochem. 103 (2009) 35.

[6] N. Poulter, M. Donaldson, G. Mulley, L. Duqye, N. Waterfield, A. G. Shard, S. Spencer, A. T, A. Junkens, A. L. Johnson. New J. Chem. 35 (2011) 1477.

[7] M. T. G. Holden, Li-Yang Hsu, K. Kurt et al. Genome Res. (2013) 1.

[8] S. Anbu, S. Kamalraj, B. Varghese, J. Muthumary, M. Kandaswamy, Inorg. Chem. 51 (2012) 5580.

[9] A. Tarushi, K. Lafazanis, J. Kljun, I. Turel, A. A. Pantazaki, G. Psomas, D. P. Kessissoglou, J. Inorg. Biochem. 121 (2013) 53.

[10] K. V. Thomas. J. Chromatogr. A 833 (1999) 105.

[11] N. L. Reeder, J. Kaplan, J. Xu, R. S. Youngquist, J. Wallace, P. Hu, K. D. Juhlin, J. R. Schwartz, R. A. Grant, A. Fieno, S. Nemeth, T. Reichling, J. P. Tiesman, T. Mills, M. Steinke, S. L. Wang, C. W. Saunders. Antimicrob. Agents Chemother. 55 (2011) 5753.

[12] C. Fernandes, A. Horn Jr, O. Vieira-da-Motta, V. M. de Assis, M. R. Rocha, L. S. Mathias, E. S. Bull, B. Szpoganicz, A. J. Bortoluzzi, E. V. Guimarães, J. C. A. Almeida,

D. H. Russell, J. Inorg. Biochem.104 (2010) 1214.

[13] I. C. Rosnizeck, M. Spoerner, T. Harsh, S. Kreitner, D. Filchtinski, C. Herrmann, D. Engel, B. König, H, R. Kalbitzer, Angew. Chem. Int. Ed. 51 (2012) 10647.

[14] T, Baines, D. Xu, C. J. Der, Future Med. Chem. 3 (2011) 1787.

[15] N. M. F. Carvalho, A. Horn Jr., A. J. Bortoluzzi, V. Drago and O. A. C. Antunes, Inorg. Chim. Acta. 359 *(*2006) 90.

[16] A. Neves, C. N. Verani, M. A. de Brito, I. Vencato, A. S. Mangrich, G. Oliva, D. D. H. F. Souza, A. A, Batista, Inorg. Chim. Acta. 290 (1999) 207.

[17] S. Striengler, M. Dittel, Inorg. Chem. 44 (2005) 2728.

[18] M. M. Ibrahim, A. M. Ramadan, G. A. M. Mersal, S. A. El-Shazly. J. Mol. Struct. 998 (2011) 1.

[19] S. S. Tandon. S. Chander, L. K. Thompson, J. N. Bridson, V. McKee, Inorg. Chim. Acta. 219 (1994) 55.

[20] Enraf-Nonius. COLLECT, Nonius BV, Delft, The Netherlands, 1998.

[21] J. M. Duisenberg, R. W. W. Hooft, A. M. M. Schreurs, J. Kroon, J. Appl. Cryst. 33 (2000) 893.

[22] A. J. M. Duisenberg, J. Appl. Cryst. 25 (1992) 92.

[23] A. J. M. Duisenberg, L. M. J. Kroon-Batenburg , A. M. M. Schreurs, J. Appl. Cryst. 36 (2003) 220.

[24] G. M. Sheldrick, *SADABS*, Program for Empirical Absorption Correction of Area Detector Data; University of Göttingen, Germany, 1996.

[25] G. M. Sheldrick, SHELXL97*Program for crystal structure refinement;* University of Göttingen, Germany, 1997.

[26] *SHELXS*-97 Direct Methods Program for Crystal Structure solution. University of

Göttingen, Germany, and refined with *SHELXL*-97 *Program for crystal structure refinement;* University of Göttingen, Germany, 1997.

[27] T. Mosmann, J. Immun. Method. 65 (1983) 55.

[28] J. H. Jorgensen, in: P. R. Murray,E. J. Baro, M. A. Pfaller, F. C. Tonover, R. H. Yolken (Eds), Manual of Clinical Microbiology, American Society of Microbiology, Washington, 1995, 1275.

[29] L. J. Farrugia, J. Appl. Cryst. 30 (1997) 565.

[30] International Tables for X-ray Crystallography. 1985, Vol. III, 270.

[31] J. Wirbser and H. Vahrenhamp, Z. Naturforsch. 1992, 47B, 962.

[32] Y. I. Kim, Y. S. Lee, H. J. Seo, J. Y. Lee, S. K. Kang, Acta. Cryst. E63 (2007) m2810.

[33] A. W. Addison, T. N. Rao, J. Reedijk, J. Van Rijn, G. C. Verschoor, J. Chem. Soc. Dalton Trans. **7** (1984) 1349.

[34] F. D. Lesh, S. S. Hindo, M. J. Heeg, M. M. Allard, P. Jain, B. Peng, L. Hryhorczuk, C. Verani, Eur. J. Inorg. Chem. 3 (2009) 345.

[35] A. Neves, I. Vencato, C. N. Verani, J. Braz. Chem. Soc. 3 (1997) 265.

[36] Z. Ma, X. Qiao, C. Xie, J. Shao, J. Xu, Z. Qiang, J. Lou, J. Inorg. Biochem. 117 (2012) 1.

[37] S. J. Riedl, Y. Shi, Nat. Rev. Mol. Cell Biol. 5 (2004) 897.

[38] M. Gurung, D. C. Moon, C. W. Choi, J. H. Lee, Y. C. Bae, J. Kim, Y. C. Lee, S. Y. Seol, D. T. Cho S. I. Kim, J. C. Lee, PLoS One. 11(6), (2011), e27958, 1.

[39] V. Sass, T. Schneider, M. Wilmes. C. Körner, A. Tossi, N. Novikova, O. Shamova, H. Sahl, Infect. Immun. 78 (2010) 2793.

[40] M. E. Selsted, A. J. Quellette, Nat. Immunol. 6 (2005) 551.

Figure Captions

Scheme 1. Scheme illustrating the synthesis of the zinc complexes **(1)-(4)**.

Figure 1. ^{1}H NMR spectra for zinc complexes: a) complex **(1),** b) complex **(2),** c) complex **(3)** and d) complex **(4)**. Each complex was dissolved in DMSO.

Figure 2.View of the *ORTEP-3* projection for **(1)** and the corresponding residue labeling scheme. Ellipsoids are shown at the 40% probability level.

Figure 3.View of the *ORTEP-3* projection for **(2)** and the corresponding residue labeling scheme. Ellipsoids are shown at the 40% probability level.

Figure 4.View of the *ORTEP-3* projection for **(3)** and the corresponding residue labeling scheme. Ellipsoids are shown at the 40% probability level.

Figure 5. Proposed structures for some signals detected in the ESI(+)-MS spectra for complexes **(2)** (left) and **(4)** (right).

Figure 6. Apoptosis induced by complex **(4)** in U-937 cells. The percentage of apoptotic cells was measured in a flow cytometer after treatment with complex **(4)** for 24 h. the cells were pre-stained with Annexin/PI. (A) Control. (B) Cisplatin – 50 µmol L^{-1}. (C) Complex **(4)** – 200 µmol L^{-1}. (D) Complex **(4)** – 400 µmol L^{-1}. Viable cells (Q3), primary apoptosis (Q4), secondary apoptosis (Q2) and necrosis (Q1).

Figure 7. Transmission electron micrograph of U937 cells after treatment with complex **(4)** at a concentration of 100 µmol L^{-1} after 6 h of incubation. N= nucleus, ER= endoplasmatic reticulum.

Figure 8. Transmission electron micrograph of U937 cells after treatment with complex **(4)** at a concentration of 200 µmol L^{-1} after 12h of incubation. M= mitochondria, ER= endoplasmatic reticulum, B= blebs, NC= nuclear chromatin, V= vacuoles.

Figure 9. Transmission electron micrograph of THP-1 cells after treatment with complex **(4)**, at a concentration of 100 µmol L^{-1} after 6 h of incubation. M= mitochondria, ER= endoplasmatic reticulum, V= vacuoles.

Figure 10. Transmission electron micrograph of THP-1 cells after treatment with complex **(4)** at a concentration of 200 µmol L^{-1} after 12h of incubation. V= vacuoles.

Figure 11. TEM of *S. aureus* cells. (A): Control; (B, C and D): after treatment with complex **(1).**

Figure 12. TEM of *S. aureus* cells. (A): Control; (B): after treatment with complex **(2).**

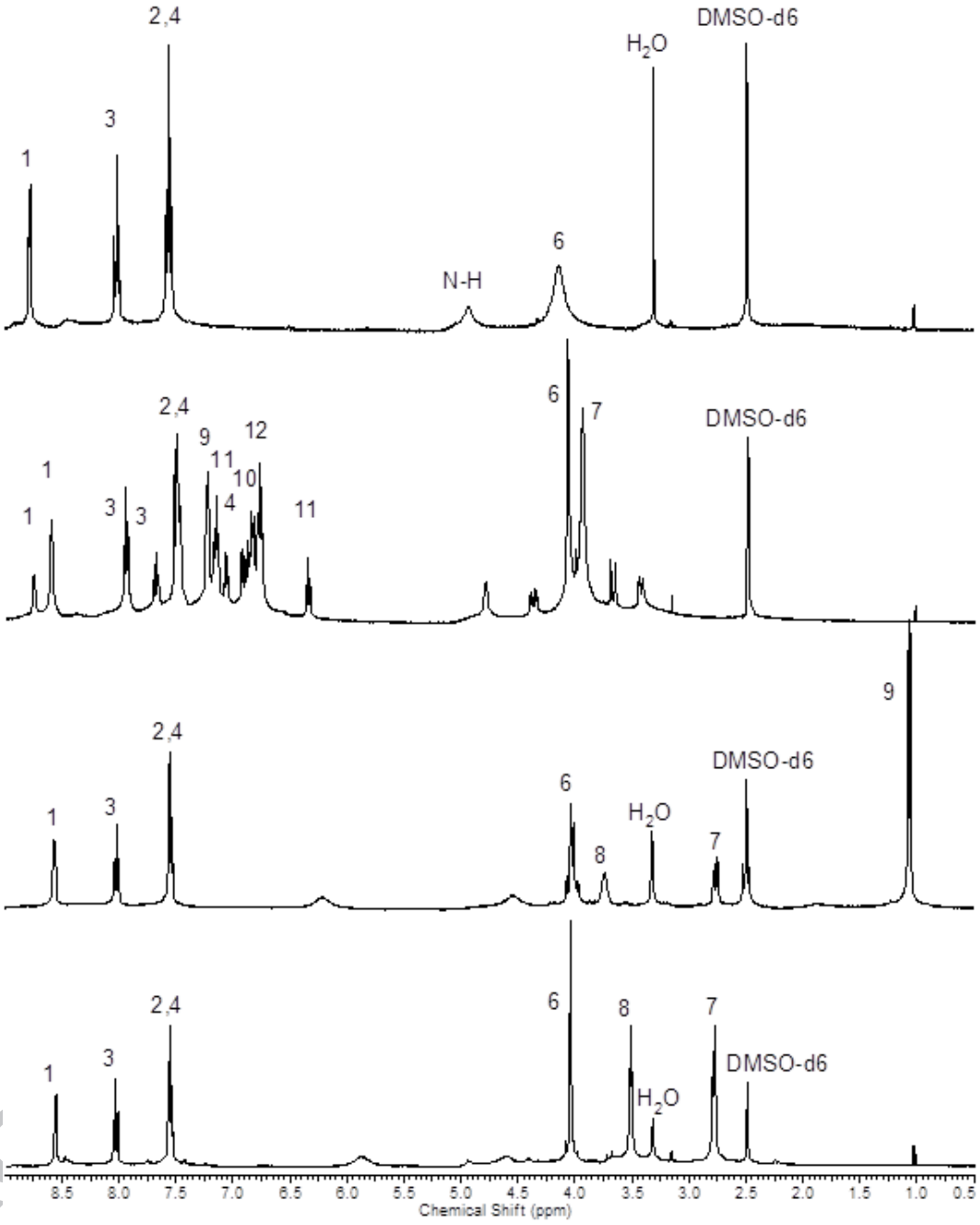

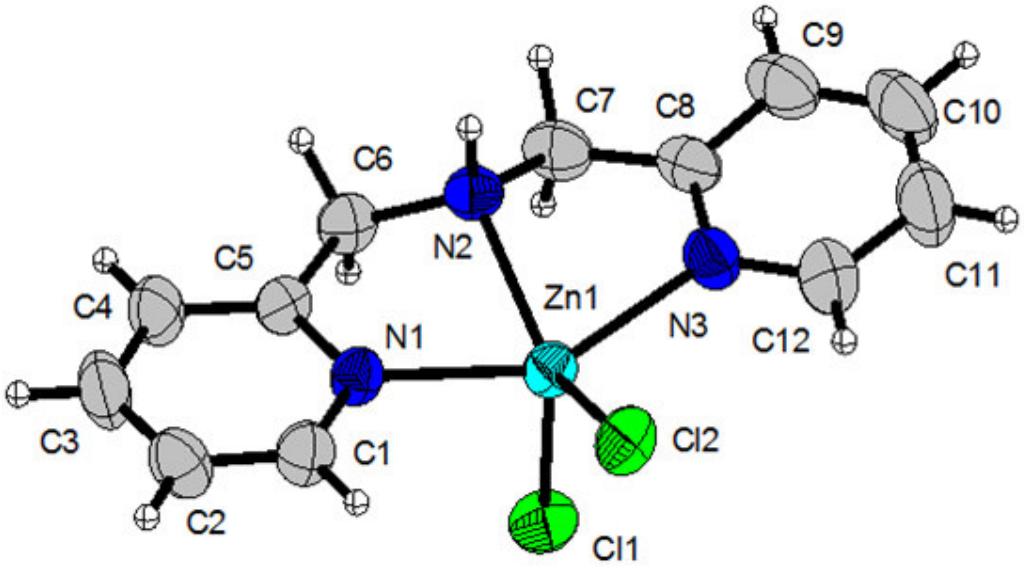

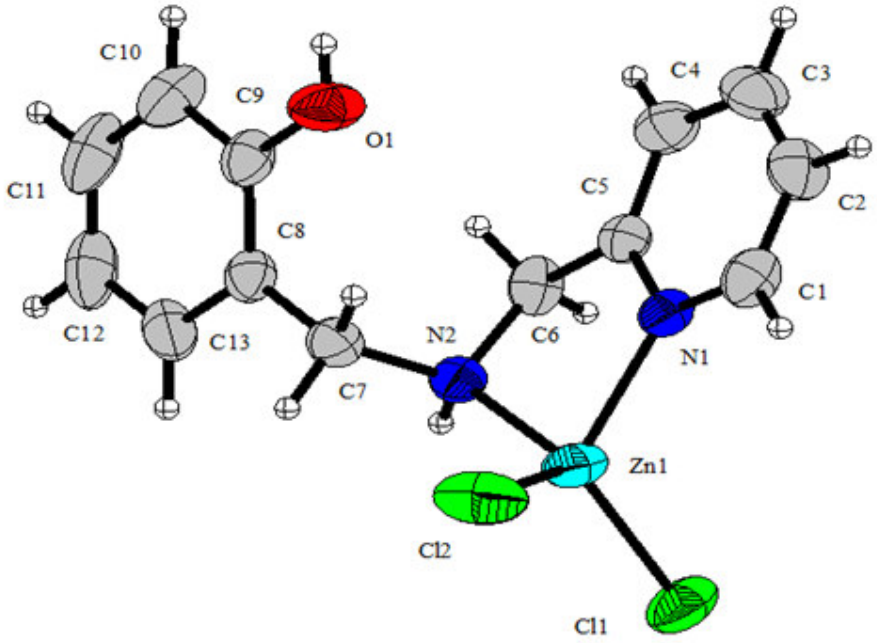

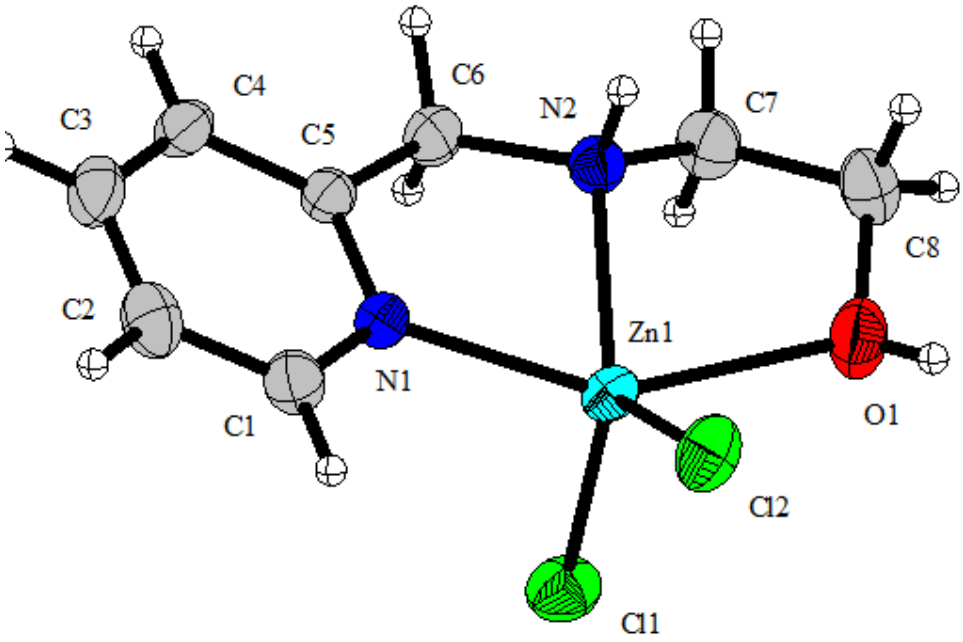

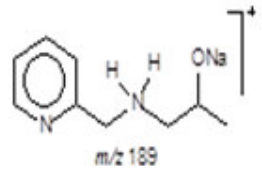

m/z 189

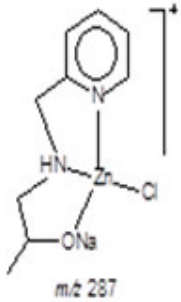

m/z 287

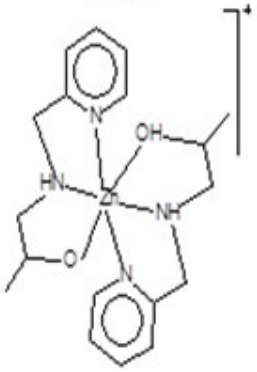

m/z 395

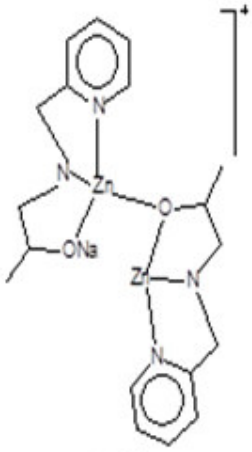

m/z 480

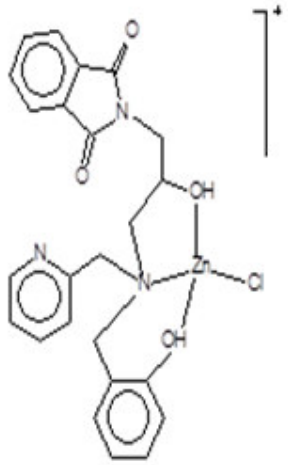

m/z 516

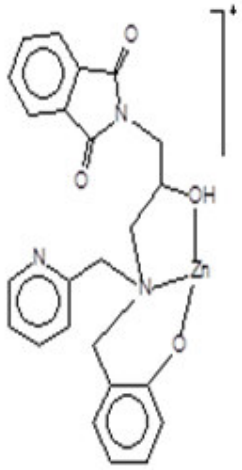

m/z 480

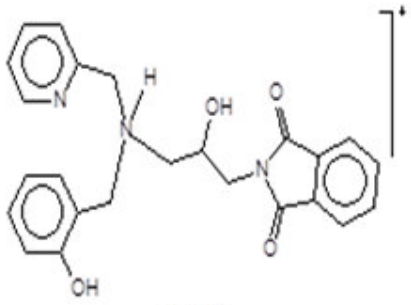

m/z 418

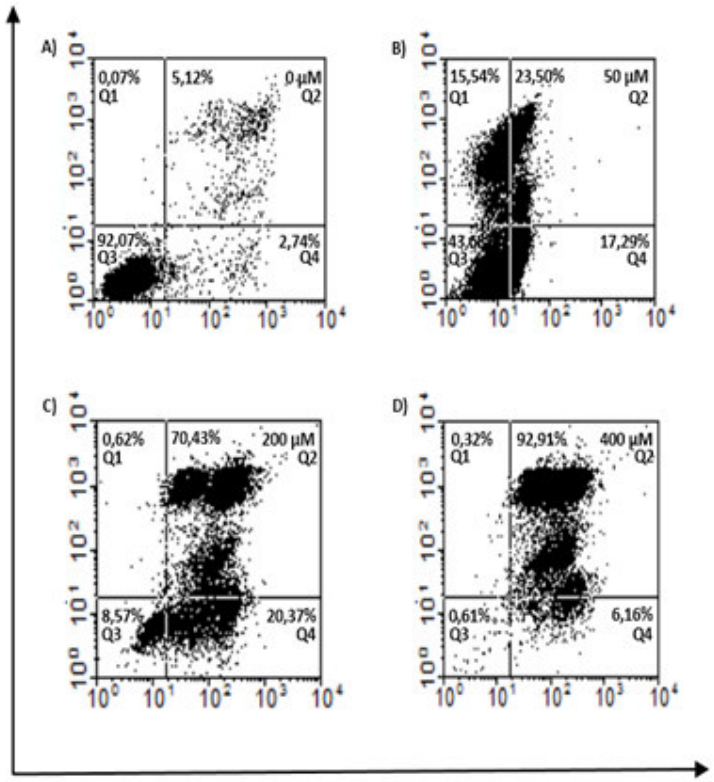

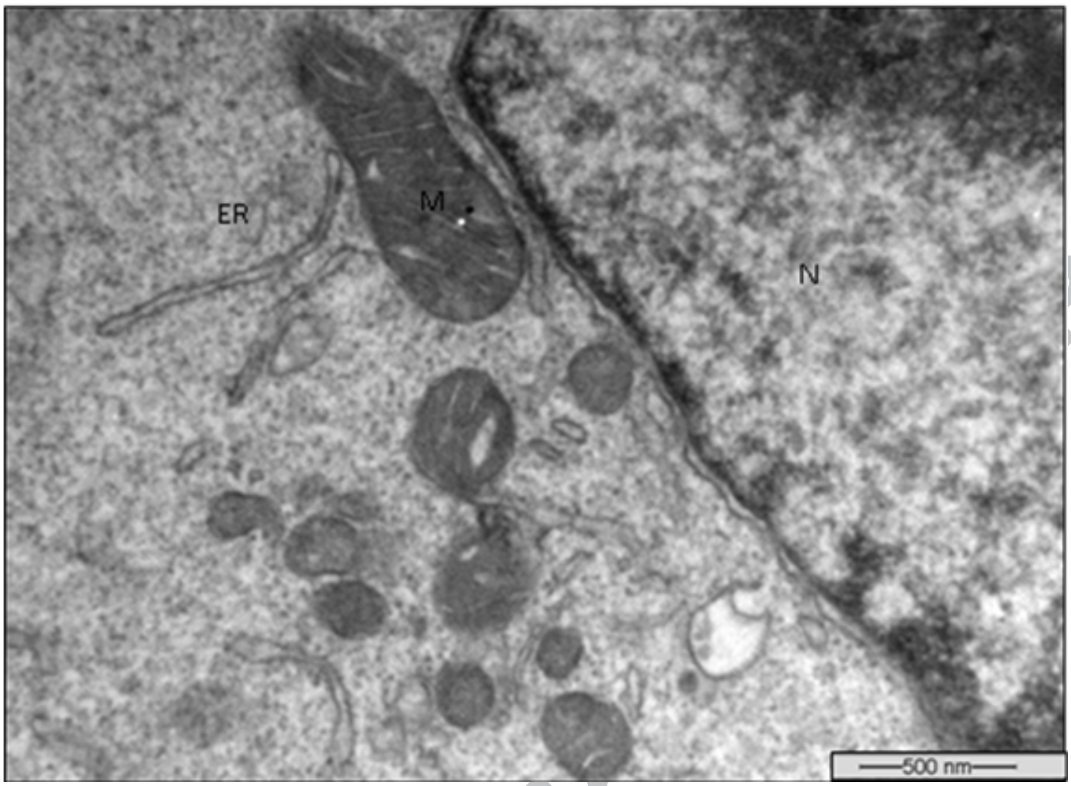

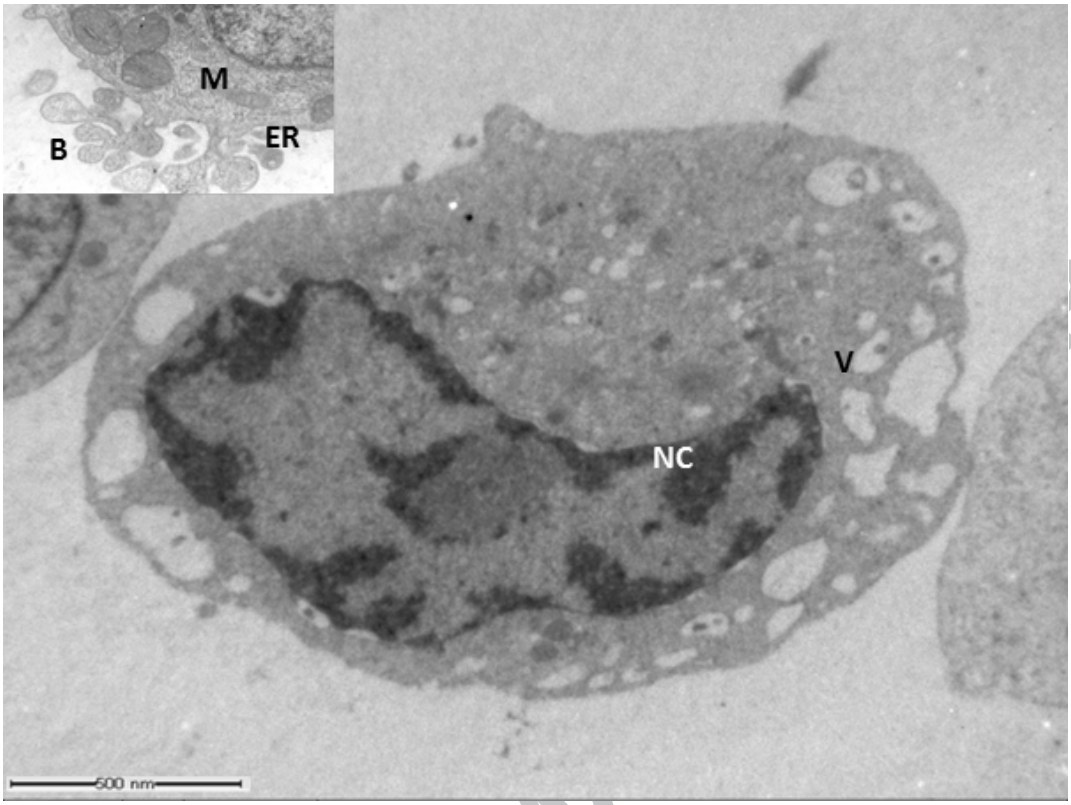

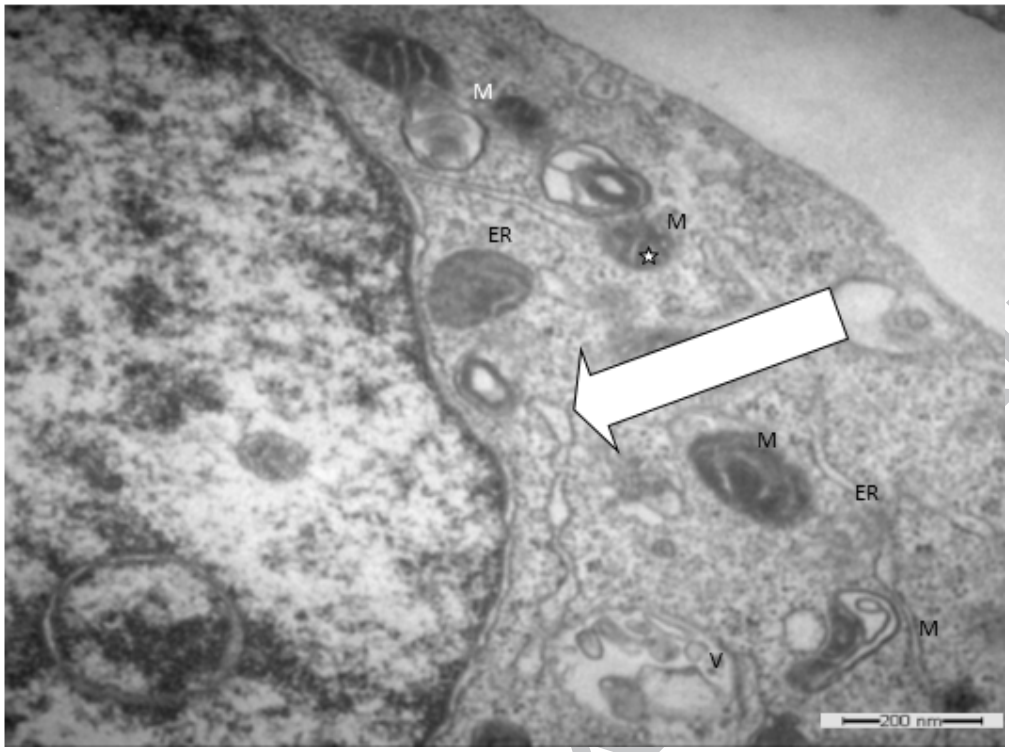

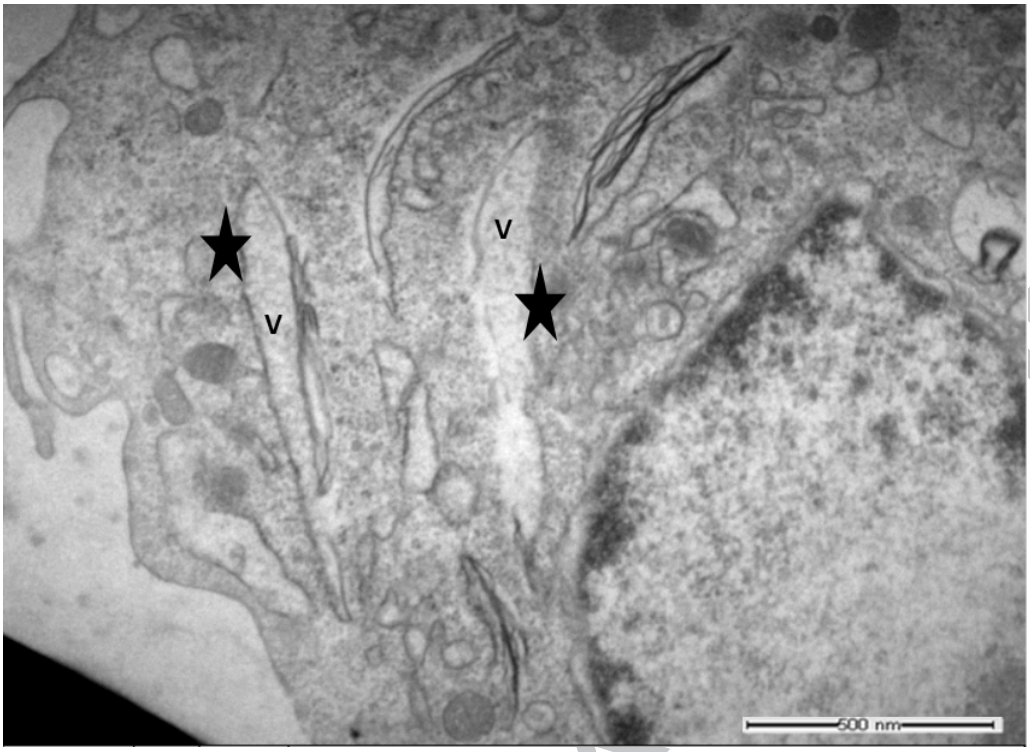

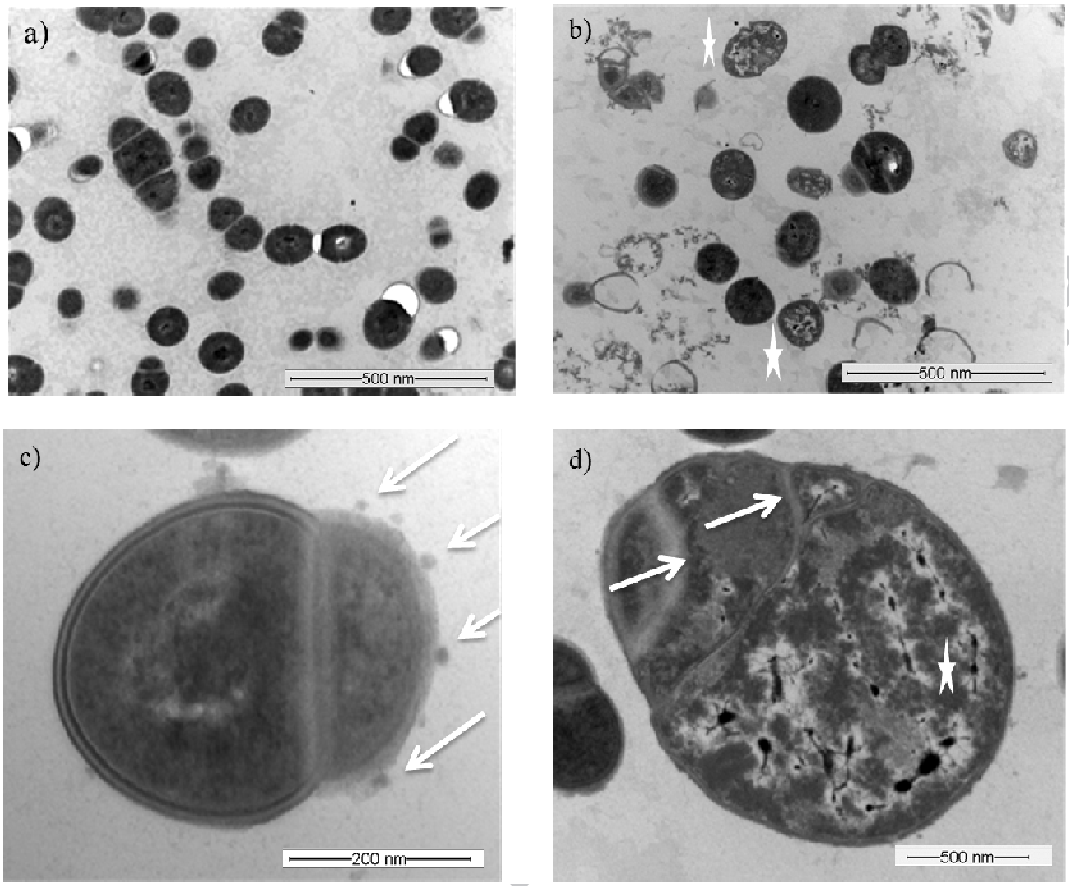

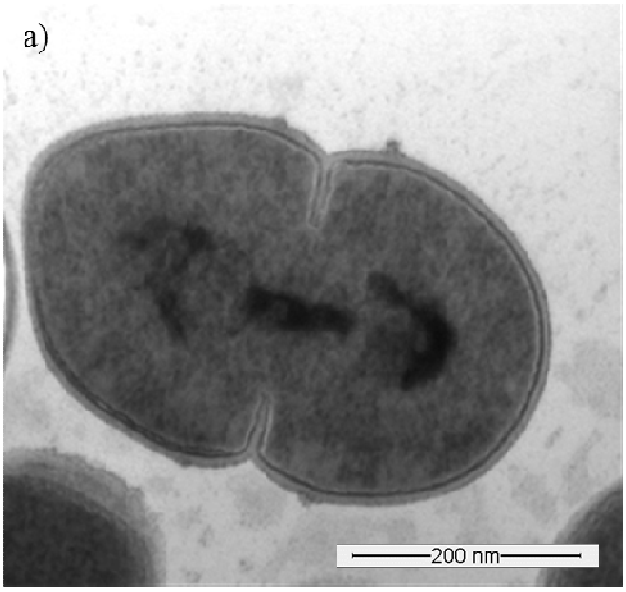

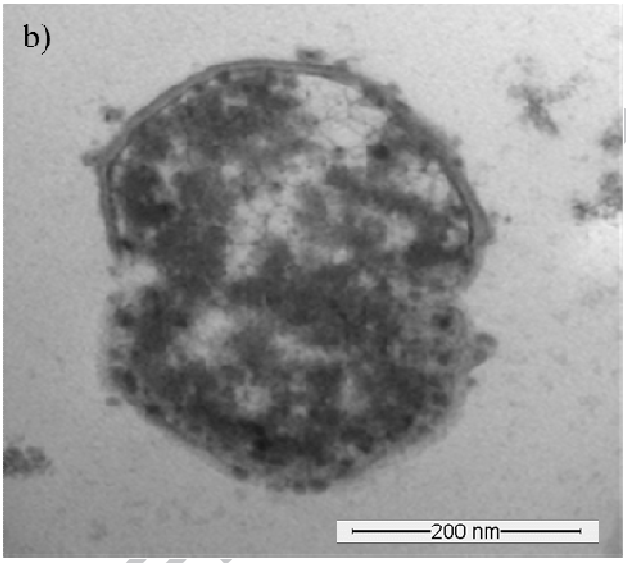

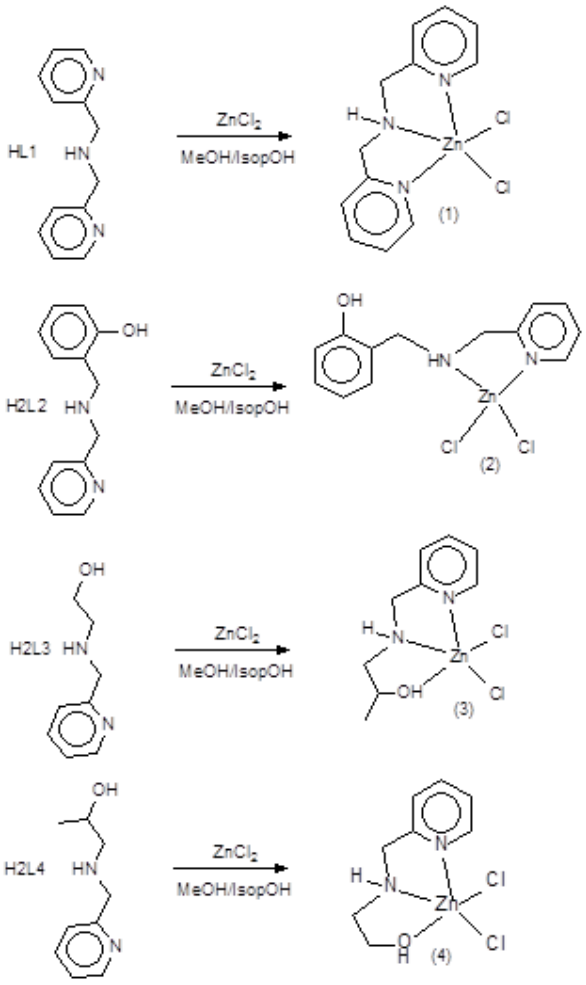

Highlights

1-Structures for the complexes were determined by X-ray diffraction and NMR.

2- Complex **(4)** shows the highest cytotoxic activity promoting cell death by apoptosis.

3- Morphological analysis of leukemia cells by TEM confirms cell death by apoptosis.

4- Complex **(2)** reaches almost100% of inhibition against three strains of *S. aureus.*

5- Morphological investigation by TEM suggests effect on bacteria cell division.

Graphical Abstract (synopsis)

Herein we present the spectroscopic and structural characterization of four new zinc complexes and biological results concerning the cytotoxic activity on human leukemia cells lines (THP-1, U937 and Molt-4) and antimicrobial activity *in vitro* against four Gram-positive bacteria (ATCC10832, ATCC25923, COL) and one animal strain *S. aureus* LSA88 (SEC/SEF/TSST-1+).

Graphical Abstract (figure)